ACS APPLIED MATERIALS & INTERFACES

Letter

www.acsami.org

CeO_2 Surface Oxygen Vacancy Concentration Governs in Situ Free Radical Scavenging Efficacy in Polymer Electrolytes

Panagiotis Trogadas, Javier Parrondo, and Vijay Ramani*

Center for Electrochemical Science and Engineering, Department of Chemical and Biological Engineering, Illinois Institute of Technology, 10 W, 33rd Street, Chicago, Illinois 60616, United States

Supporting Information

ABSTRACT: Nonstoichiometric CeO_2 and $Ce_{0.25}Zr_{0.75}O_2$ nanoparticles with varying surface concentrations of Ce^{3+} were synthesized. Their surface Ce^{3+} concentration was measured by XPS, and their surface oxygen vacancy concentrations and grain size were estimated using Raman spectroscopy. The surface oxygen vacancy concentration was found to correlate well with grain size and surface Ce^{3+} concentration. When incorporated into a Nafion polymer electrolyte membrane (PEM), the added nonstoichiometric ceria nanoparticles effectively scavenged PEM-degradation-inducing free radical reactive oxygen species (ROS) formed during fuel cell operation. A 3-fold increase in the surface oxygen vacancy concentration resulted in an order of magnitude enhancement in the efficacy of free radical ROS scavenging by the nanoparticles. Overall, the macroscopic PEM degradation mitigation rate was lowered by up to 2 orders of magnitude using nonstoichiometric ceria nanoparticles with high surface oxygen vacancy concentrations

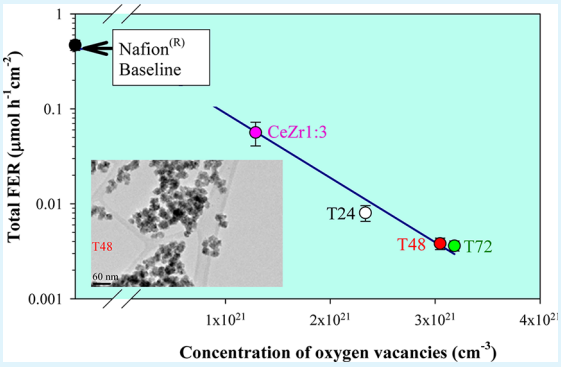

KEYWORDS: *reactive oxygen species, free radical scavenging, PEM degradation, nonstoichiometric cerium oxide*

Cerium oxide has attracted much attention because of its numerous technological applications. It has been used (1) as an active catalyst in vehicle emission systems for oxidation of pollutant gases,[1,2] (2) as an electrolyte material for solid oxide[3,4] and proton exchange membrane fuel cells,[5,6] (3) as an electrode material for gas sensors for monitoring environmental pollution,[7,8] (4) in silicon-on-insulator structures,[9,10] (5) in superconducting field effect devices,[11] (6) in ultraviolet absorbents,[12] and (7) in high-temperature oxidation resistant coatings.[13] Many of those applications arise from the facility of the Ce^{3+}/Ce^{4+} redox couple and the high mobility of nonstoichiometry-induced oxygen vacancies in nanosized ceria materials.[14]

Recent research using X-ray photoelectron spectroscopy (XPS) and X-ray absorption near edge structure (XANES) suggests that the concentration of Ce^{3+} relative to Ce^{4+} as well as the lattice constant in ceria increases as particle size decreases.[15,16] The presence of dual oxidation states implies that the oxide is nonstoichiometric, and that the oxide lattice has oxygen vacancies.[17] The observed size dependence of lattice nonstoichiometry suggests that the number of surface vacancies will be larger at smaller particle sizes.[18] The oxygen vacancies, created to maintain charge neutrality in the lattice, increase the ease with which the material can absorb and release lattice oxygen.[14]

There have been numerous studies on polymer electrolyte fuel cell (PEFC) durability that have shown that the components of the central membrane electrode assembly (MEA), especially the polymer electrolyte membrane (PEM), deteriorate during long-term operation.[19−21] As described elsewhere, PEM degradation modes can be classified as thermal (desulfonation, solvolysis), mechanical (pinhole and crack formation) and chemical (free radical induced oxidative degradation).[19] Among these modes, PEM chemical degradation is reported to be a major contributor to PEFC lifetime limitations. The chemical degradation of the PEM occurs in a two-step process: (i) formation of reactive oxygen species (ROS) such as hydroxyl (HO•) and hydroperoxyl (HOO•) radicals; and (ii) reaction of ROS with the PEM leading to chain scission as well as release of fluoride from the backbone/side chain.[20] The rate at which fluoride is released from the PEM backbone (fluoride emission rate; FER) can be readily measured and provides a macroscopic estimate of the PEM degradation rate.

Endoh and co-workers[22] and Coms and co-workers[23] were the first to propose and demonstrate the use of cerium and manganese ions to reduce fluoride emission rate (FER) in PEM during fuel cell operation. The metal ions function as fast, efficient and reversible scavengers of free radicals formed during fuel cell operation. Although these ions were not immobilized and had some negative effects on the ionic conductivity and/or

Received: August 9, 2012
Accepted: September 21, 2012
Published: September 21, 2012

   dx.doi.org/10.1021/am3016069 | ACS Appl. Mater. Interfaces 2012, 4, 5098−5102

activity of the electrodes, the addition of these ions reduced the FER by 2−3 orders of magnitude.

Previous work from this group,[5,6] has demonstrated that the incorporation of nonstoichiometric CeO_2 nanoparticles within a recast Nafion membrane resulted in greater than an order of magnitude reduction in the FER observed during accelerated PEM degradation tests. This mitigation in PEM degradation was attributed to the effective scavenging of free radical ROS by the nonstoichiometric oxide − this hypothesis was confirmed by using in situ fluorescence spectroscopy to monitor ROS generation and capture within the PEM in an operating PEFC.[24] Briefly, the mechanism of free radical scavenging in CeO_2 revolves around the multiple oxidation states of the metal ion.[25,26] The harmful HO• can be scavenged by lattice oxygen vacancy sites, resulting in the concomitant oxidation of Ce^{3+} to Ce^{4+}. Once Ce^{3+} gets oxidized through reaction with HO•, there is a mechanism for its regeneration (and hence vacancy regeneration) on the surface of ceria nanoparticles in acidic environments.[27]

The following reactions have been proposed for free radical scavenging and Ce^{3+} regeneration:[23]

During free radical scavenging, the surface Ce^{3+} is oxidized to Ce^{4+} as follows

$$HO\bullet + Ce^{3+} + H^+ \rightarrow Ce^{4+} + H_2O \quad (1)$$

During CeO_2 regeneration, surface Ce^{4+} is reduced back to Ce^{3+} on the surface of ceria by the following reactions

$$Ce^{4+} + H_2O_2 \rightarrow Ce^{3+} + HOO\bullet + H^+ \quad (2)$$

$$Ce^{4+} + HOO\bullet \rightarrow Ce^{3+} + O_2 + H^+ \quad (3)$$

$$2Ce^{4+} + H_2 \rightarrow 2Ce^{3+} + 2H^+ \quad (4)$$

$$4Ce^{4+} + 2H_2O \rightarrow 4Ce^{3+} + 4H^+ + O_2 \quad (5)$$

Note that hydrogen and water are readily available on the membrane.

The ratio of Ce^{3+}/Ce^{4+} in the lattice and thereby the concentration of oxygen vacancies is therefore an important parameter for tuning the free radical scavenging activity of ceria. This ratio can be tuned by controlling the size of ceria nanoparticles, or by the incorporation of other elements in the ceria lattice to enhance the formation of oxygen vacancies.[14] It has been reported that the stability of the ceria microstructure and its oxygen storage capacity is improved by doping it with suitable cations such as Zr^{4+}, Al^{3+}, or Si^{4+}.[28,29]

The present study investigates the relationship between Ce^{3+} surface concentration, surface oxygen vacancy concentration, and the free radical scavenging properties of CeO_2 and $Ce_{0.25}Zr_{0.75}O_2$. On the basis of the above discussion, it is hypothesized that an increase in surface Ce^{3+} concentration will enhance surface oxygen vacancy concentration in the lattice, which in turn should enhance the free radical scavenging ability of ceria-based materials. To test this hypothesis, we synthesized ceria and ceria-zirconia nanoparticles with varying surface Ce^{3+} concentrations (and hence different surface oxygen vacancy concentrations), and characterized and incorporated them within the PEM. The surface Ce^{3+} concentration was tuned by controlling ceria particle size[30] or by doping the lattice with zirconia.[29] The efficacy of the added nonstoichiometric oxide nanoparticles in mitigating ROS-induced PEM oxidative degradation was investigated as a function of the oxygen vacancy concentration at the oxide surface. The FER was used as a macroscopic estimate of PEM degradation rate in these studies.

The Ce^{3+} concentration at the surface of each oxide was calculated by fitting the experimental X-ray photoelectron spectroscopy (XPS) spectra; values obtained are compiled in Table 1. The spectra obtained and details of the calculations are presented in the Supporting Information (Table S1, Figure S1; affiliated discussion].

Table 1. Concentration of Ce^{3+} on the Surface of CeO_2 and $Ce_{0.25}Zr_{0.75}O_2$ Nanoparticles

sample ID	sample	Ce^{3+} surface concentration (mol %) from XPS
T24	CeO_2 (24 h reaction)	8.8
T48	CeO_2 (48 h reaction)	10.3
T72	CeO_2 (72 h reaction)	10.0
CeZr1:3	$Ce_{0.25}Zr_{0.75}O_2$	3.2

Samples T48 and T72 exhibited similar surface Ce^{3+} concentration of approximately 10 mol %, whereas samples T24 and CeZr1:3 had lower surface Ce^{3+} concentrations of 8.8 mol % and 3.2 mol %.

Raman spectroscopy was used to estimate the grain size of the oxide and the concentration of oxygen vacancies (defect concentration) at the surface of the ceria and ceria-zirconia nanoparticles.[31−34] The microstructure of CeO_2 is known to influence the shape of Raman spectrum. The Raman-active mode of nanoceria corresponds to a frequency of 458 cm^{-1} (Figure 1) instead of 466 cm^{-1}, the characteristic frequency of

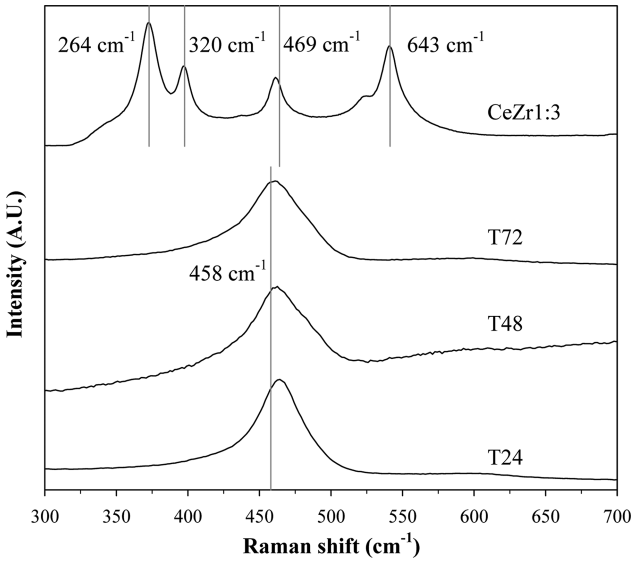

Figure 1. Raman spectra of CeO_2 (obtained under different reaction times) and $Ce_{0.25}Zr_{0.75}O_2$ nanoparticles.

microceria.[35] The feature observed at this frequency is assigned to the symmetrical stretching mode of Ce−O8 vibrational unit.[31,32] The Raman spectrum of $Ce_{0.25}Zr_{0.75}O_2$ revealed 4 strong Raman peaks (Figure 1): (i) at 264 and 320 cm^{-1}, originating from the six Raman active modes ($A_{1g} + 2B_{1g} + 3E_g$) of tetragonal ZrO_2,[36] (ii) at 469 cm^{-1}, due to the F_{2g} Raman active mode of cubic CeO_2[31,32] and (iii) at 643 cm^{-1}, attributed to the presence of oxygen vacancies in the $Ce_{0.25}Zr_{0.75}O_2$ surface structure.[35,37]

dx.doi.org/10.1021/am3016069 | ACS Appl. Mater. Interfaces 2012, 4, 5098−5102

The Raman line (~466 cm^{-1}) broadening can be described by the dependence of its half width at half-maximum (HWHM) on the grain size. HWHM increased with decreasing grain size from 12.5 cm^{-1} for CeZr3:1 to 23.4 cm^{-1} for T72. Grain size (d_g) and HWHM (Γ) are inter-related by the correlation proposed by Weber and co-workers[33]

$$\Gamma(cm^{-1}) = 5 + 51.8/d_g(nm) \quad (6)$$

The concentration of oxygen vacancies was estimated using the spatial correlation model from the relationship between correlation length and grain size[31,33,38,39]

$$L(nm) = \sqrt[3]{\left(\frac{\alpha}{2d_g}\right)^2 [(d_g - 2\alpha)^3 + 4d_g^2\alpha]} \quad (7)$$

Where L is correlation length (average distance between two lattice defects), and α the radius of CeO_2 units (0.34 nm), determined from universal constants.[31] The defect concentration N (cm^{-3}) can be calculated from the correlation length L (nm) as a function of grain size:[31,33]

$$N = 3/4\pi L^3 \quad (8)$$

Figure 2 shows the oxygen vacancy concentration of the samples prepared as a function of their grain size. CeO_2 samples

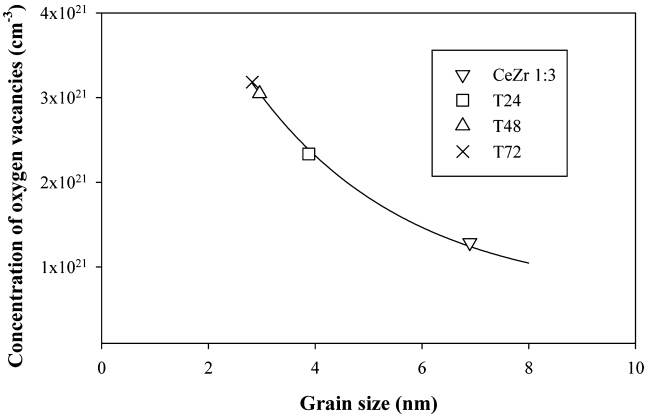

Figure 2. Concentration of oxygen vacancies as a function of grain size.

T48 and T72 had the highest concentration of oxygen vacancies on their surface (~3 × $10^{21}cm^{-3}$) as well as the lowest grain size, confirming that the lower the grain size of the nanoparticle, the higher the defect concentration on the surface. In general, the oxygen vacancy concentration increased with the surface Ce^{3+} concentration (Figure 3).

Accelerated degradation tests were performed in an operating PEFC to estimate the scavenging activity of the different ceria and ceria-zirconia materials when added to the PEM. To monitor the macroscopic PEM degradation rate, we tested membrane electrode assemblies (MEAs) prepared using the ceria/ceria-zirconia additive-infused PEMs in a fuel cell test station at open circuit at 90 °C and 30% relative humidity. Polarization curves were also obtained under varying current/voltage conditions to evaluate the effect of the additives on the fuel cell performance (the experimental details and the results obtained can be found in the Supporting Information). Oxygen (0.2 SLPM) was used as the oxidant at the cathode and hydrogen (0.2 SLPM) was used as the fuel at the anode. The

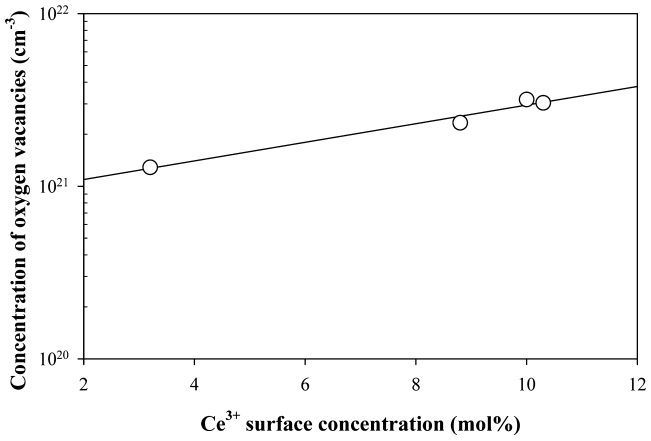

Figure 3. Concentration of oxygen vacancies as a function of Ce^{3+} surface concentration.

test was run for 24–48 h and the effluent water in the anode and cathode streams were condensed in cold-traps. The fluoride ion concentration in the condensate water was measured using a fluoride ion selective electrode. These data, in conjunction with the condensation rate of water, were used to calculate the fluoride emission rate (FER) from the MEA and hence quantify the macroscopic rate of PEM degradation. Each experiment was repeated at least 4 times to quantify the experimental error.

The mean FERs (with accompanying standard error) are reported in Figure 4 for all the MEAs tested. Two conclusions

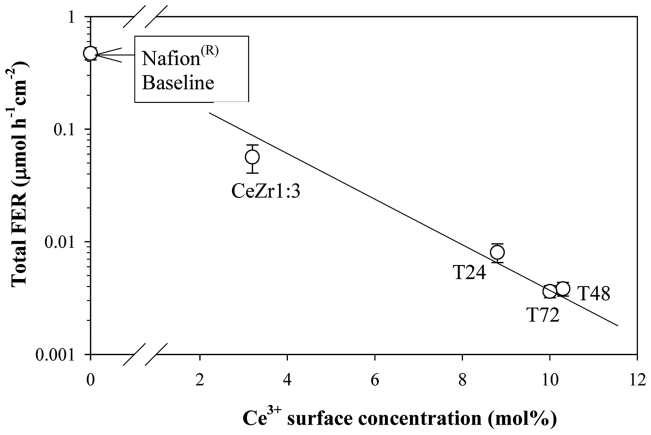

Figure 4. Macroscopic rate of composite membrane degradation (in an operating fuel cell) as a function of Ce^{3+} surface concentration of the added oxide. CeO_2 loading: 0.15 mg/cm^2 membrane.

can be readily drawn from an inspection of Figure 4: (1) the addition of CeO_2 and $Ce_{0.25}Zr_{0.75}O_2$ to Nafion resulted in a substantial (close to or greater than 1 order of magnitude) reduction in the total FER, and hence the total macroscopic PEM degradation rate, compared to a baseline MEA prepared with unmodified recast Nafion; and (2) the decrease in FER tracked very well with the Ce^{3+} surface concentration (and the oxygen vacancy concentration) in the added oxide. The observed trend provided direct validation of the governing hypothesis. These results illustrate the importance of regenerative oxygen vacancies on the surface structure of CeO_2 in determining the ability of ceria-based additives to scavenge free radicals within the PEM and to thereby mitigate

dx.doi.org/10.1021/am3016069 | ACS Appl. Mater. Interfaces 2012, 4, 5098–5102

PEM degradation. These results can also be translated to other applications where the ceria is used as free radical scavenger, or as an agent to store oxygen within the lattice.

EXPERIMENTAL SECTION

To synthesize ceria nanoparticles, we independently prepared and mixed hexamethylenetetramine (0.5 M) and cerium nitrate (0.5M) solutions for varying length of time (24, 48, and 72 h) to obtain ceria with different particle sizes.[30] Hexamethylenetetramine hydrolyses slowly to produce ammonia, resulting in a slow and homogeneous increase in the pH of the solution, and in the precipitation of small nanoparticles of CeO_2 with a narrow size distribution.[30] The final product was recovered by centrifugation, washed with DI water and dried at 60 °C.

For the preparation of $Ce_{0.25}Zr_{0.75}O_2$ nanoparticles, cerium nitrate (18.4 mmol) and zirconyl chloride (55.4 mmol) were dissolved in 400 mL DI water (pH ∼ 10−11). Ammonium hydroxide (90 mL, 2 M) was slowly added to the solution, and the mixture was stirred overnight. The resulting suspension was filtered to recover the precipitate, which was washed with DI water and dried at 60 °C. Finally, the powder was heated at 800 °C for 2 h (in air atmosphere) to get the mixed oxide.[40] The nomenclature used to describe the samples is shown in Table 1.

Composite membranes used in the durability study were prepared by addition of metal oxide nanoparticles to 5 wt % Nafion (1100 EW) dispersion, maintaining the loading of additive constant at 3 wt % (dry weight of the ionomer). The suspension was stirred and casted onto a glass plate, followed by drying at 60 °C. Baseline recast Nafion membranes without any additive were prepared for comparison.

Membrane electrode assemblies (MEAs) used in the accelerated durability tests had an active area of 5 cm^2. The electrodes were applied by spraying a slurry comprising Pt/C (40 wt % Pt, Alfa Aesar), Nafion dispersion, and methanol onto both sides of the PEM using an airbrush. The overall loading of platinum on each electrode was maintained at 0.4 ± 0.05 mg cm^{-2}.

The Raman spectra were recorded from 100 to 1200 cm^{-1} using a Renishaw Ramascope 2000. X-ray photoelectron spectroscopy was done using an XPS spectrometer model Axis 165 (Kratos Analytical, Shimadzu Co.), with a monochromatic X-ray source of MgKα.

ASSOCIATED CONTENT

Supporting Information

Detailed experimental methods, XPS Peak fitting, and TEM. This material is available free of charge via the Internet at http://pubs.acs.org.

AUTHOR INFORMATION

Corresponding Author

*E-mail: ramani@iit.edu.

Notes

The authors declare no competing financial interest.

ACKNOWLEDGMENTS

This work was supported by an IIT start-up research grant.

REFERENCES

(1) Steele, B. C. H. *Solid State Ionics* **1984**, *12*, 391−406.
(2) McCarty, J. G.; Wise, H. *Catal. Today* **1990**, *8*, 231−248.
(3) Mogensen, M.; Sammes, N. M.; Tompsett, G. A. *Solid State Ionics* **2000**, *129*, 63−94.
(4) Eguchi, K.; Setoguchi, T.; Inoue, T.; Arai, H. *Solid State Ionics* **1992**, *52*, 165−172.
(5) Trogadas, P.; Parrondo, J.; Ramani, V. *Electrochem. Solid-State Lett.* **2008**, *11*, B113−B116.
(6) Trogadas, P.; Parrondo, J.; Ramani, V. *ACS Symp. Ser.* **2010**, *1034*, 187−207.
(7) Martinelli, G.; Carotta, M. C.; Ferroni, M.; Sadaoka, Y.; Traversa, E. *Sens. Actuators, B* **1999**, *B55*, 99−110.
(8) Jasinski, P.; Suzuki, T.; Anderson, H. U. *Sens. Actuators, B* **2003**, *B95*, 73−77.
(9) Chikyow, T.; Bedair, S. M.; Tye, L.; El-Masry, N. A. *Appl. Phys. Lett.* **1994**, *65*, 1030−1032.
(10) Morshed, A. H.; Moussa, M. E.; Bedair, S. M.; Leonard, R.; Liu, S. X.; El-Masry, N. *Appl. Phys. Lett.* **1997**, *70*, 1647−1649.
(11) Walkenhorst, A.; Schmitt, M.; Adrian, H. *Appl. Phys. Lett.* **1994**, *64*, 1871−1873.
(12) Tsunekawa, S.; Sivamohan, R.; Ohsuna, T.; Kasuya, A.; Takahashi, H.; Tohji, K. *Mater. Sci. Forum* **1999**, *315−445*, 315−317.
(13) Patil, S.; Kuiry, S. C.; Seal, S. *Proc. R. Soc. London, Ser. A.* **2004**, *460*, 3569−3587.
(14) Babu, S.; Thanneeru, R.; Inerbaev, T.; Day, R.; Masunov, A. E.; Schulte, A.; Seal, S. *Nanotechnology* **2009**, *20*, 085713.
(15) Tsunekawa, S.; Fukuda, T.; Kasuya, A. *Surf. Sci.* **2000**, *457*, L437−L440.
(16) Zhang, F.; Wang, P.; Koberstein, J.; Khalid, S.; Chan, S.-W. *Surf. Sci.* **2004**, *563*, 74−82.
(17) Robinson, R. D.; Spanier, J. E.; Zhang, F.; Chan, S.-W.; Herman, I. P. *J. Appl. Phys.* **2002**, *92*, 1936−1941.
(18) Deshpande, S.; Patil, S.; Kuchibhatla, S. V. N. T.; Seal, S. *Appl. Phys. Lett.* **2005**, *87*, 133113.
(19) LaConti, A. B.; Hamdan, M.; McDonald, R. C., State-of-the-art performance and durability. In *Handbook of Fuel Cells: Fundamentals, Technology, and Applications*; Vielstich, W.; Gasteiger, H. A.; Lamm, A., Eds.; John Wiley & Sons: New York, 2003; Vol. 3, pp 647−662.
(20) Chen, W.; Sun, G.; Guo, J.; Zhao, X.; Yan, S.; Tian, J.; Tang, S.; Zhou, Z.; Xin, Q. *Electrochim. Acta* **2006**, *51*, 2391−2399.
(21) Luo, Z.; Li, D.; Tang, H.; Pan, M.; Ruan, R. *Int. J. Hydrogen Energy* **2006**, *31*, 1831−1837.
(22) Endoh, E.; Terazono, S.; Widjaja, H.; Takimoto, Y. *Electrochem. Solid-State Lett.* **2004**, *7*, A209−A211.
(23) Coms, F. D.; Liu, H.; Owejan, J. E. *ECS Trans.* **2008**, *16*, 1735−1747.
(24) Prabhakaran, V.; Arges, C. G.; Ramani, V. *Proc. Natl. Acad. Sci.* **2012**, *109*, 1029−1034.
(25) Chung, D. *NewScientist* **2003**, *179*, 2410−2416.
(26) Schubert, D.; Dargusch, R.; Raitano, J.; Chan, S.-W. *Biochem. Biophys. Res. Commun.* **2006**, *342*, 86−91.
(27) Tsunekawa, S.; Sivamohan, R.; Ito, S.; Kasuya, A.; Fukuda, T. *Nanostruct. Mater.* **1999**, *11*, 141−147.
(28) Colon, G.; Pijolat, M.; Valdivieso, F.; Vidal, H.; Kaspar, J.; Finocchio, E.; Daturi, M.; Binet, C.; Lavalley, J. C.; Baker, R. T.; Bernal, S. *J. Chem. Soc., Faraday Trans.* **1998**, *94*, 3717−3726.
(29) Potdar, H. S.; Deshpande, S. B.; Deshpande, A. S.; Gokhale, S. P.; Date, S. K.; Khollam, Y. B.; Patil, A. J. *Mater. Chem. Phys.* **2002**, *74*, 306−312.
(30) Zhang, F.; Jin, Q.; Chan, S.-W. *J. Appl. Phys.* **2004**, *95*, 4319−4326.
(31) Kosacki, I.; Suzuki, T.; Anderson, H. U.; Colomban, P. *Solid State Ionics* **2002**, *149*, 99−105.
(32) Suzuki, T.; Kosacki, I.; Anderson, H. U.; Colomban, P. *J. Am. Ceram. Soc.* **2001**, *84*, 2007−2014.
(33) Weber, W. H.; Hass, K. C.; McBride, J. R. *Phys. Rev. B: Condens. Matter* **1993**, *48*, 178−185.
(34) Kaspar, J.; Fornasiero, P.; Balducci, G.; Di, M. R.; Hickey, N.; Sergo, V. *Inorg. Chim. Acta* **2003**, *349*, 217−226.
(35) Patil, S.; Seal, S.; Guo, Y.; Schulte, A.; Norwood, J. *Appl. Phys. Lett.* **2006**, *88*, 243110.

(36) Fernandez, L. E.; Sanchez, E. V.; Panizza, M.; Carnasciali, M. M.; Busca, G. *J. Mater. Chem.* **2001**, *11*, 1891−1897.
(37) Fujii, M.; Nagareda, T.; Hayashi, S.; Yamamoto, K. *Phys. Rev. B: Condens. Matter* **1991**, *44*, 6243−6248.
(38) Parayanthal, P.; Pollak, F. H. *Phys. Rev. Lett.* **1984**, *52*, 1822−1825.
(39) Tiong, K. K.; Amirtharaj, P. M.; Pollak, F. H.; Aspnes, D. E. *Appl. Phys. Lett.* **1984**, *44*, 122−124.
(40) Reddy, B. M.; Khan, A.; Yamada, Y.; Kobayashi, T.; Loridant, S.; Volta, J.-C. *Langmuir* **2003**, *19*, 3025−3030.